# Recent Advances of Pico-Tesla Resolution Magneto-Impedance Sensor Based on Amorphous Wire CMOS IC MI Sensor

T. Uchiyama[1], K. Mohri[2], *Life Fellow, IEEE*, Y. Honkura[3], and L. V. Panina[4]

[1]Graduate School of Engineering, Nagoya University, Nagoya 464-8603, Japan
[2]Nagoya Industrial Science Research Institute (NISRI), Nagoya 464-0819, Japan
[3]Aichi Steel Corportation, Tokai 476-8666, Japan
[4]Plymouth University, Plymouth, U.K.

We have developed sensitive micro magnetic sensors referred to as MI sensors based on magneto-impedance effect in amorphous wires and CMOS IC electronic circuits providing a sharp-pulse excitation. Micro sized MI-HIC chips have been in mass production of electronic compasses by Aichi Steel Corp. since 2002 for mobile phones and since 2010 for smart phones. Recently we have realized pico-Tesla ($10^{-8}$ Oe) resolution for micro MI sensors making use of ultralow intrinsic magnetic noise in amorphous wires with the pulse magnetoimpedance effect. The pico-Tesla MI sensor is useful especially for bio-magnetic measurements without any magnetic shielding at room temperature. In order to avoid a risk of traffic accident due to noise reduction electric vehicles, an alert system for the pedestrians having a smart phone would be useful, if pico-Tesla MI sensor were built in the smart phones.

*Index Terms*—Biomagnetic field, electronic compass, magnetoimpedance sensor, magnetoencephalogram (MEG), pico-tesla resolution, spine.

## I. INTRODUCTION

W E have found the magneto-impedance effect in amorphous wires in 1993 [1]–[14] and invented new sensitive micro magnetic sensors referred to as "MI sensor" based on a pulse-current magneto-impedance effect in amorphous wires and CMOS IC sensor electronic circuitry in 1997 [15]. Since then, the sensor operation has been considerably improved in terms of stability using an analog switch [16]. Based on these achievements, Aichi Steel Company successfully developed micro MI sensors for mobile phone electronic compasses [17]–[26].

We have summarized three principal advantageous features of the amorphous wire MI sensor [24]–[26] as:

1) submillimeter size sensor head is realized with a high sensitivity of several nT resolution. Thus, we designed 3-axis electronic compass chips having 0.4 mm length with 10 $\mu$m diameter amorphous wire heads, compatible with the advanced integrated circuitry for smart phones, in which a power consumption is around 0.8 mW [24];

2) ultrahigh sensitivity with a resolution of 1 pT without any magnetic shielding in a portable type MI sensor operating at room temperature [27]–[33];

3) ultraquick response for magnetic field signal frequencies ranging from 0 to several GHz [10].

The three features are based on the magnetoimpedance effect originated from the skin effect in amorphous wires with a circular domain structure as illustrated in Fig. 1. for the pulse-current magnetoimpedance, the magnetization dynamics in such amorphous wire is limited by the magnetization rotation in the
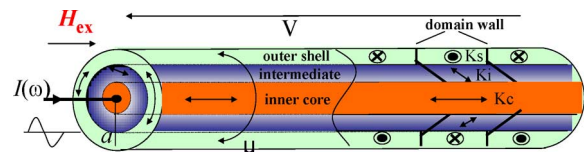
Fig. 1. Domain structure of amorphous wire. Circular domains exist in the outer region and the inner core has an axial magnetization. The driving ac current I($\omega$) generates a circular magnetic field, response to which is characterized by the circumferential (transverse) permeability $\mu$. This response is highly sensitive to the applied magnetic field H$_{ex}$, and could be measured as a voltage V induced across the wire ends.

surface layer (outer layer region). Thus, the magnetization processes in the inner core are not generated, avoiding strong demagnetizing fields against an external axial magnetic field and magnetic noises due to fluctuation of spike domains. There is also no limitation on frequency or rising time of a magnetizing pulse current (apart from the condition of a strong skin effect), resulting in ultraquick response of the MI sensor.

The principal expression of the Magneto-Impedance effect in amorphous wires is as follows:

$$Z = (1/2)R_{dc} k\alpha J_0(k\alpha)/J_1(k\alpha)$$
$$= (\alpha/2)R_{dc}(2\rho)^{-1/2}(1+j)(\omega\mu_\theta)^{1/2}$$
$$k = (1-j)/\delta \quad \text{for } \delta(=(2\rho/\omega\mu_\theta)^{1/2}) \ll \alpha. \quad (1)$$

Magnetoimpedance sensitivity is expressed as

$$\partial Z/\partial Hex$$
$$= (\alpha/4)\omega^{1/2}R_{dc}(2\rho\mu_{\theta 0})^{-1/2}(1+j)\partial\mu_\theta/\partial Hex \quad (2)$$

where R$_{dc}$ is the wire dc resistance, J$_0$, J$_1$ are the Bessel functions of the 0-order and 1st-order.

Fig. 2 illustrates progression of the MI sensor projects classified in three groups depending on sensor applications: micro size compatible with integrated circuitry, ultrahigh sensitivity
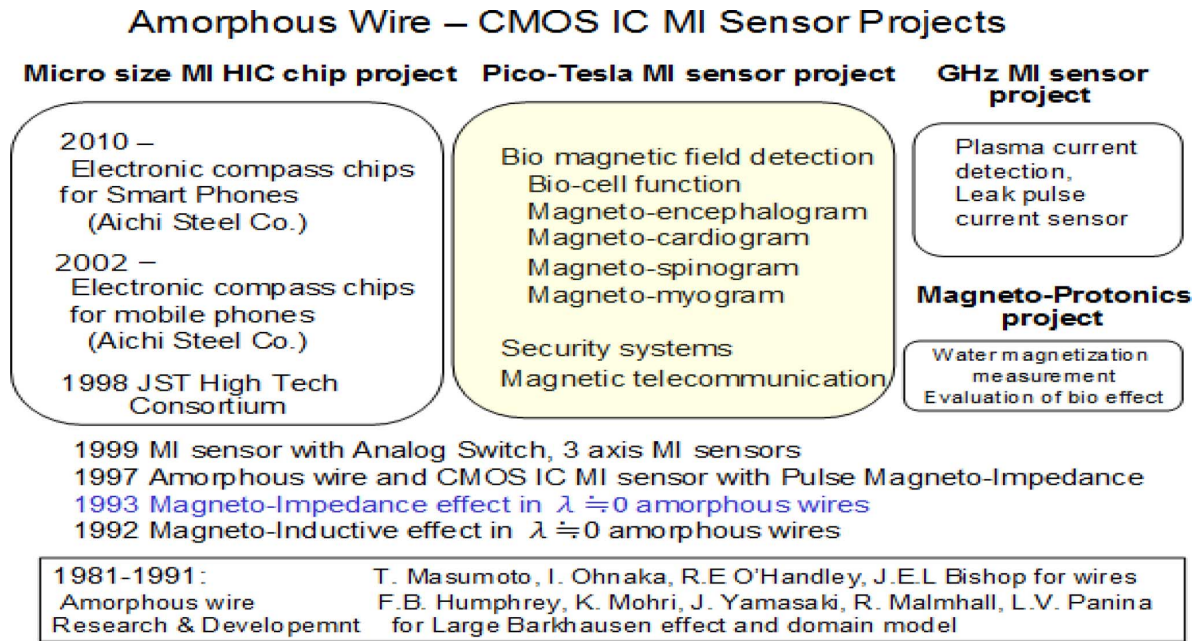
Fig. 2. Amorphous wire and CMOS IC MI sensor projects based on three principal advantageous features.

with 1 pico-Tesla resolution and portability, and ultraquick response.

## II. PICO-TESLA RESOLUTION MI SENSORS

### A. Basic Electronic Circuitry of a Linear MI Sensor

We have constituted highly sensitive linear micro magnetic-field sensors (MI sensors) inventing the pulse magnetoimpedance effect for tension-annealed amorphous wires with wound pick-up coils, combined with the CMOS IC multivibrator circuit [15], [16], [20]–[24].

The pick-up coil is wound on a zero magnetostrictive (slightly negative $\lambda = -10^{-7}$) tension annealed amorphous CoFeSiB wire of 30 $\mu$m in diameter (a-wire) for constitution of highly linear magnetic sensors. The tension annealing makes the magnetization in the surface layer (the outer shell domain) laying along the circumferential (transversal) direction. For such magnetic configuration, the voltage induced in the pick-up coil is zero if no magnetic field is applied and increases linearly with the field. A principle MI sensor electronic circuit for magnetic-field detection is shown in Fig. 3. The square-wave voltage generator (multivibrator: LMC555) produces a rectangular voltage train. The differential circuit (R1, C1) transfers the square wave voltage into a positive sharp pulse. The current pulse train, with a width $\tau$ and a time interval $T$, is applied to the a-wire as a carrier using CMOS inverter (74AC04). The dc component (average amount) of the current pulse train removes the domain walls in the outer shell realizing a single domain and greatly reducing the magnetic noise and the hysteresis of magnetic-field sensing. A strong skin effect for the pulse magneto-impedance in a-wire is insured due to a quick rising time of around 100 ns. Thus, such pulse excitation does not lead to any magnetization in the inner core domain generating spike domain fluctuation magnetic noises. For a helical static magnetization induced with a dc magnetic field applied along the a-wire length
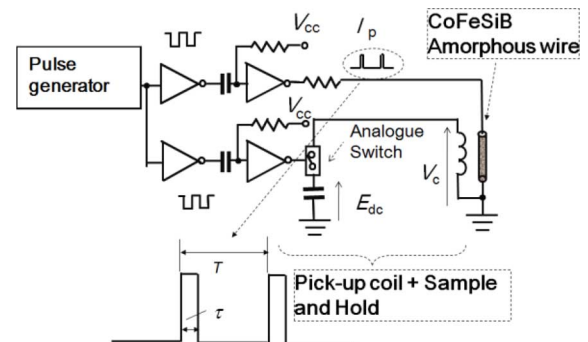


Fig. 3. Basic electronics for magnetic field sensor. A linear MI sensor based on the pulse magneto-impedance in an amorphous wire with pickup coil. $I_p$ is pulse current to magnetize the amorphous wire element and $V_c$ is an induced voltage at the pick-up coil.

direction, the pulse current $i$ passing through the wire induces a coil pulse voltage $V_c$ the height of which in the first pulse only is proportional to the applied dc magnetic field $H_{ex}$. The analog switch (SW:74HC4066) picks up only the first pulse in the induced voltage waveform cutting following noise oscillatory wave, and also stabilizes the sensor circuit operation with its inner resistance. The first pulse is converted to a dc voltage $E_{dc}$ using a low-pass filter circuit.

In this experiment, we use a pulse current having the values of $\tau$ and $T$ of 100 ns and 2.5 $\mu$s, respectively. Considering the peak value of the current pulse $I_p$ of approximately 100 mA, the dc bias current $I_b = (\tau/T)I_p$ is estimated to be 4 mA. This $I_b$ generates circumferential dc bias filed $H_b(= I_b/2\pi a)$ of 42 A/m, that is larger than the circumferential coercive force of CoFeSiB a-wires [24]. Therefore, the circumferential bias magnetic field could eliminate circular domain structure to decrease magnetic noise due to wall motion. It has been pointed out that
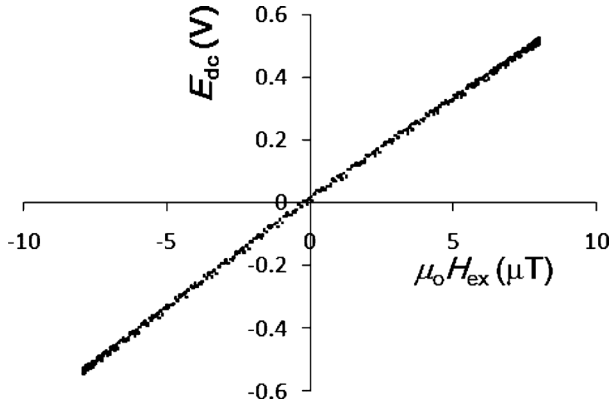
Fig. 4. $E_{dc}$ versus $H_{ex}$ characteristics of the MI sensor. Number of turns of the pickup coil is 300 and the length of the wire is 1 cm.
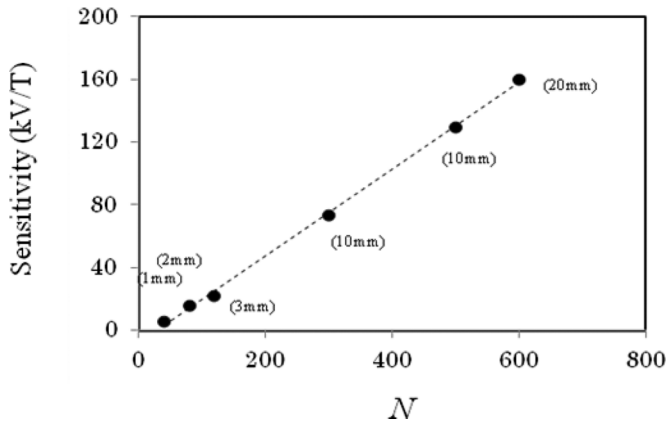


Fig. 5. Sensitivity dependence on number of pickup coil turns $N$ for a linear MI sensor after rectification. The wire length for each experiment is given inside the round brackets.
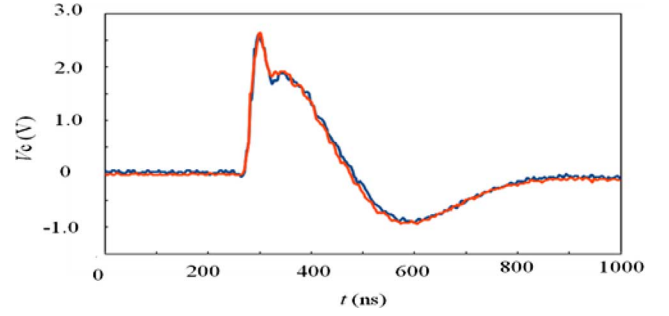


Fig. 6. Induced voltage in the sensing coil (red line) and that in the reference coil (blue line). The length of amorphous wire element is l cm and the number of turns of a pickup coil is 500.
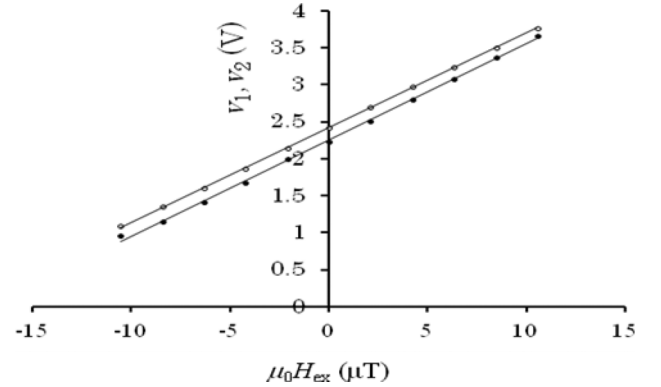


Fig. 7. Field detection characteristics of two pick up coils wound on an amorphous wire for gradiometer. Open and close circles indicate the sensing coil rectification voltage $v_1$ and reference coil rectification voltage $v_2$, respectively.

the intrinsic magnetic field noise spectral density of the MI element within a simplified model for single domain structure is expressed as [34]

$$\beta = \sqrt{\frac{2\alpha k_B T}{\gamma M_s \pi a^2 l}}$$

where $T$ is the temperature, $\alpha$ is the magnetic damping constant, $k_B$ is Boltzman constant, $\gamma$ is the gyro magnetic ratio, $M_s$ is the saturation magnetization, $a$ is the diameter and $l$ is the length of a wire element. Using typical parameters for Co-rich a-wires, we could estimate the value of $\beta$. If magnetic noise is measured over a band width of 1 Hz, a 1 cm length wire yields $\beta$ of approximately 10 fT at the room temperature [34]. In other words, the best possible resolution of the MI sensor for magnetic field detection is in the range of a fT level (except the electronic circuit noises).

The field detection characteristics of MI sensor due to coil pickup voltage are shown in Fig. 4. The length of the wire is 1 cm and the number of coil turns is 300. A very high field detection sensitivity of about 66 kV/T and good linearity are obtained.

The sensitivity dependence on number of turns $N$ is shown in Fig. 5. The wire length for each experiment is given inside the round brackets. The normalized sensitivity estimated from

the slope of sensitivity vs. $N$ characteristics is 249 V/T/turns. In general, a high sensitivity in the range of 100 kV/T is expected for a pico-tesla resolution magnetic field sensor. If we detect 1 pT magnetic field with the help of the element having the sensitivity of 100 kV/T, the sensing element yields a 100 nV signal. Assuming the frequency band of the system to be 100 Hz, the signal of 100 nV corresponds to the voltage noise of the instrumental amplifier having noise spectral density of 10 nV/Hz$^{1/2}$. Furthermore, various background magnetic fields such as the geomagnetic field and electric generator fields are additional magnetic noises to sensor circuit noise that decrease the signal-to-noise ratio in measurements. Therefore, the high sensitivity of MI sensor given by (2) along with minimized circuit noises and other noises (common-mode noises, normal-mode noises and radiation noises) should be realized to achieve pico-Tesla resolution without any magnetic shielding.

### B. MI Gradiometer

In order to detect very weak magnetic field such as a biomagnetic field, we constructed MI gradiometer for the cancellation of background uniform noises such as the geomagnetic field. For this sensor head, the a-wire has two coils: a sensing coil and a reference coil. The distance between the two pick up coils is set to be 3 cm. The induced coil voltages $V_c$ from two pick up coils are shown in Fig. 6. Two voltage waveforms well coincide with each other. Fig. 7 illustrates the field detection characteristics using a 500- turns pick up coil, where $v_1$ is the rectified
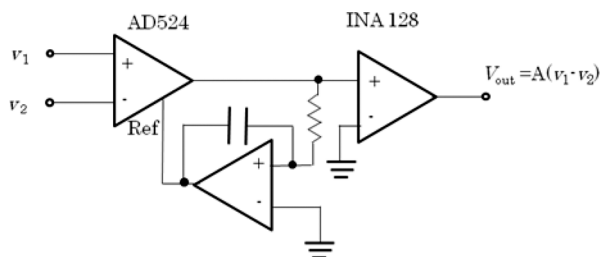
Fig. 8. Diagram of the amplification circuit with auto-zero negative feedback for MI gradiometer. The analogue integrator is used for nulling the input offset voltage.
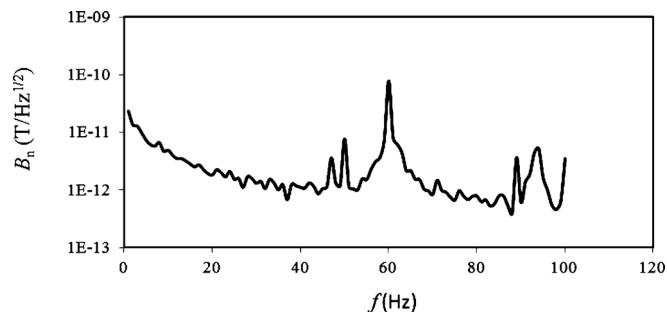


Fig. 10. Frequency characteristics of MI gradiometer for biomagnetic measurement.



Fig. 9. Noise spectral density for MI gradiometer without any magnetic shied. After the subtraction voltage $v_d$ is amplified using an instrumentation amplifier ($A = 10\,000$), the data are analyzed by a laptop computer.



Fig. 11. Experimental set up for the magnetic measurement at back of the head. The MI sensor is set to measure the magnetic field $B_x$ perpendicular to back plane with the spacing d = 5 mm.



Fig. 12. Magnetic field from the back left side of the head in (a) and back ground noise in (b). The eyes were opened during the first 8 s and then closed during the following 8 s.

voltage from the sensing coil and $v_2$ is from the reference coil. The sensitivity of the sensing coil is 130 kV/T and the difference in sensitivity between $v_1$ and $v_2$ is within 1.5%. If a subtraction voltage $v_d = v_1 - v_2$ is used as an output voltage, the influence of a uniform background magnetic field can be almost neglected. When a local magnetic field (signal) is applied at the position of the sensing coil, the subtraction voltage $v_d$ becomes proportional to the local field.

The signal amplification circuit diagram for gradiometer is shown in Fig. 8. In order to obtain a stable and high gain amplification, the auto-zero circuit due to a negative feedback is employed. Fig. 9 illustrates the noise spectral density of the MI gradiometer without any shielding. The operating frequency of the noise measurement is from 0.3 to 100 Hz. After the subtraction voltage $v_d$ is amplified using an instrumentation amplifier ($A = 10\,000$), the data are analyzed by a laptop computer. The sampling rate and resolution of the AD convert system were 1 ms and 14 bits, respectively. It is noted that the noise level of less than 10 pT/Hz$^{1/2}$ is achieved for frequencies from 2 to 20 Hz and nearly 1 pT/Hz$^{1/2}$ from 20 to 40 Hz. Fig. 10 illustrates the designed frequency response of the MI gradiometer using band pass filter and notch (band illumination) filter for the purpose of biomagenetic field measurement.

## III. APPLICATIONS

### A. Biomagentic Measurement

We have tried to measure magnetoencephalogram (MEG) using the pico-tesla resolution (pT) MI sensor under no shield environment. The experimental set up for magnetic field measurement at back of the head is shown in Fig. 11. The sensor is set to measure 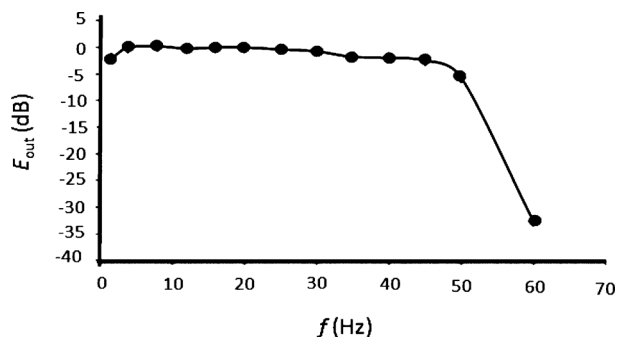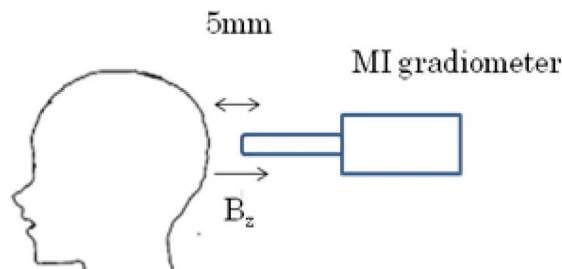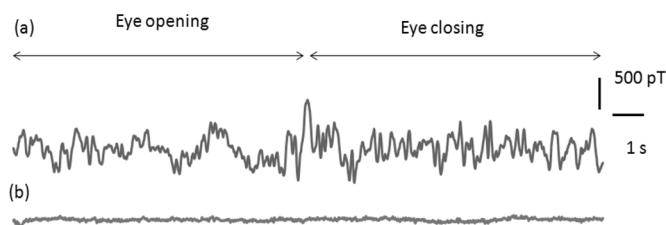a magnetic field $B_x$ perpendicular to the back plane with the spacing d = 5 mm. Fig. 12 illustrates the measurement results of time series of magnetic field for a seated 50 years old man in comparison with background noise. The eyes were opened during the first 8 s and then closed during the following 8 s. It is shown that the magnetic signal intensity from the back of the head is more than ten times larger than that of the background noise. According to the time series of magnetic field in Fig. 12(a), an alpha wave component (8–13 Hz) seems to be enhanced after eyes are closed. In order to confirm the activation of the alpha wave component due to eyes closing, we analyzed the frequency spectrum of the MEG. Fig. 13 illustrates the time dependence of $\alpha/\beta$, where $\alpha$ is partial over all of alpha wave in magnetic field and $\beta$ is partial over all of beta wave (14–30 Hz) in magnetic field. It is clear that the ratio $\alpha/\beta$ is increased after eyes closing.

An advance measurement of a magnetic field from the spinal cord has been attempted using a SQUID magnetometer [35], [36]. Recently, we have demonstrated that a biomagnetic field at the spine position can be measured using pT MI sensor as well
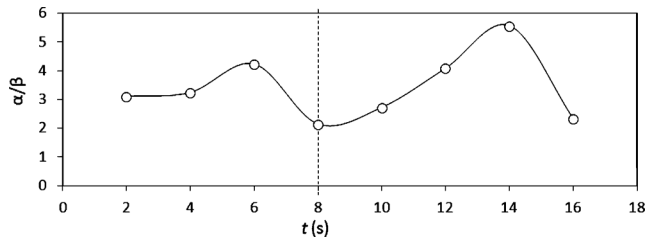
Fig. 13. Time dependence of $\alpha/\beta$, where $\alpha$ is partial over all of the alpha wave (8–13 Hz) and $\beta$ is partial over all of the beta wave (14–30 Hz) in magnetic field at back of the head.
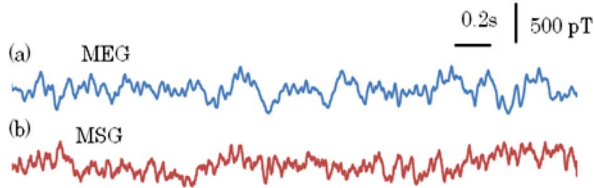


Fig. 14. Simultaneously measured magnetic fields at the back of the head in (a) and at the spine position in (b) A subject quietly lies on his back for avoidance of influence of the myogram on a flat wooden bed with eyes closing and two pT-MI gradiometer were set in a bed slit just under the position near the spin and back of the head.
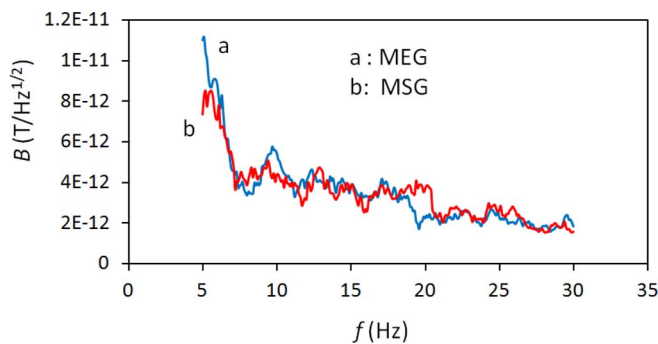


Fig. 15. Spectrum analysis of both MEG and MSG for simultaneously measured data with the use of pT-MI sensor. Both MEG and MSG have similar frequency components.
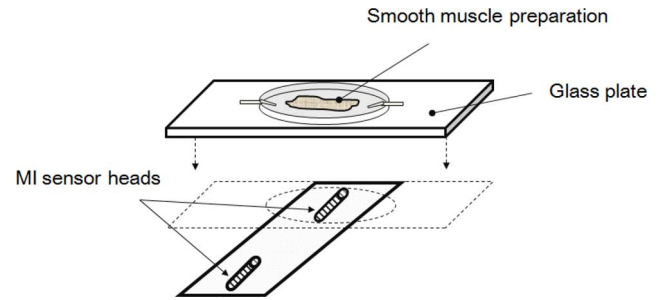


Fig. 16. Experimental setup for measuring the active magnetic field in smooth muscle preparations, which are dipped in the a circulating wormed physiological saline solution.
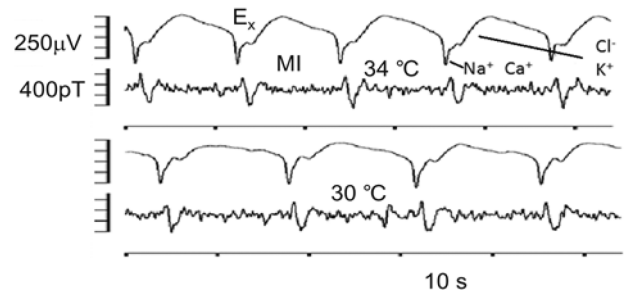


Fig. 17. Measured results of simultaneously detected time series of the electric and magnetic oscillatory signals for a guinea-pig stomach preparation.

as MEG. Fig. 14 illustrates the results of simultaneous measurement of magnetic fields using a pair of pT MI sensors at the back of the head (MEG) in (a) and at the spine (thoracic) position (MSG) in (b). A subject quietly lies on his back for avoidance of influence of the myogram on a flat wooden bed with eyes closed and two pT-MI gradiometer were set in a bed slit just under the position near the spin and back of the head for the non-contact measurement. It appears to be some similarity between MEG and MSG due to presence of a similar frequency component. The frequency spectra for both magnetic fields of MEG and MSG are shown in Fig. 15. For that reason, we may expect to detect magnetic field due to neural activity of the spine position using pT MI sensor. We have been successful to evaluate the arousal effect caused by a physiological magnetic stimulation using MSG signals for several subjects [28], [33].

The biomageitic field in the living cell tissue has been also investigated using pT-MI sensor. Fig. 16 illustrates the experimental setup for the bio-magnetic field detection for a

living tissue, which is dipped in a circulating wormed physiological saline solution during the measurement. We have used a stomach musculature of the guinea pig as the preparation, which produces pace making electric activity with a rather regular cycle even after isolation. The results of simultaneously detected time series of the electric and magnetic oscillatory signals are shown in Fig. 17. $E_x$ reflects the extracellular electrical field along the longitudinal direction of preparations so that $E_x$ is proportional to the extracellular current flow. The sharp pulse waveform is considered to be due to $Na^+$ - $Ca^{2+}$ exchange flow through the membrane ion channels and the slow recovering parts are due to $K^+$ and $Cl^-$ flow. The changes in the magnetic field precisely synchronized with the extracellular electric activity. It seems that these two activities provide different biological information. A phase lag of around 2 s of the magnetic signal pulse against the electric signal pulse is found, which is considered to be due to a time lag of the ion flow on the tissue surface and the ion flow inside the tissue.

### B. Other Applications

Hybrid cars are so quiet when operating in electric mode (EV mode) that they may pose a risk to the blind, small children, the elderly, runners, cyclists, and other pedestrians. A hybrid car is needed to be 74 percent closer than a conventional car when people could hear sounds and recognize from which direction the car is approaching [37].

The photograph of the hybrid car (Toyota Prius) detection experiment using mobile type pT-MI sensor is shown in Fig. 18(a), and the detected magnetic signal from the Prius at a distance of 4 m is shown in Fig. 18(b). The frequency of the ac magnetic
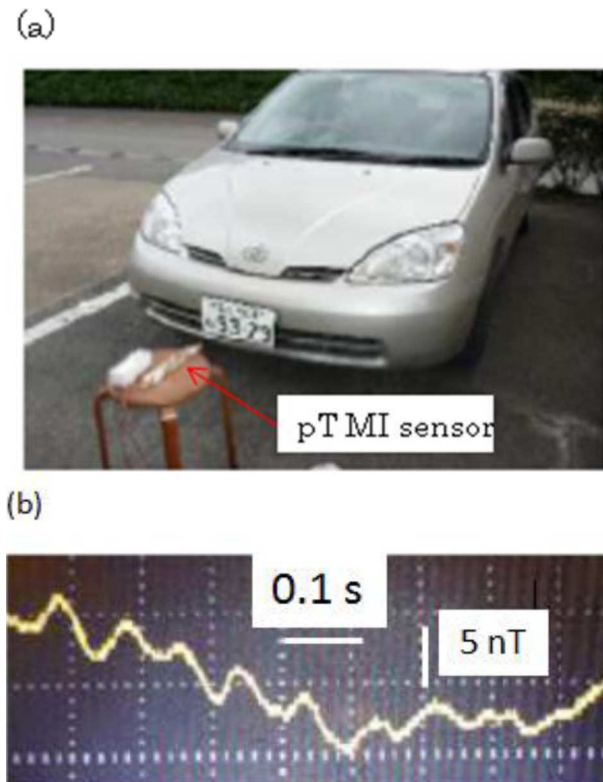
(a)



(b)

Fig. 18. A hybrid car detection experiment using mobile type pT MI sensor. The experimental set up is shown in (a) and detected magnetic field in (b). The frequency of the ac magnetic field is 11 Hz and amplitude of the field is from 2 to 5 nT.

field is 11 Hz and the amplitude of the field is from 2 to 5 nT. It is estimate that pT-MI sensor can detect the approaching electric vehicles from the distance of around 10 m. In order to avoid a risk of traffic accident due to noise reduction electric vehicles, an alert system for the pedestrians having a smart phone would be useful, if pT-MI sensor were built in smart phones.

Various reliable security sensor systems such as MRI accident protection, antishop lifting, and underground navigation system are under development using the pT MI sensors. The pT MI sensors are also available for person-to-person direct magnetic telecommunications as hearing assistance for elderly.

## IV. Conclusion

We have newly developed pico-Tesla ($10^{-8}$ Oe) resolution micro magnetic sensors using the amorphous wire and CMOS IC circuit on the basis of intrinsic ultralow magnetic noises in amorphous wires with the pulse Magneto-Impedance effect. The pico-Tesla MI sensor is useful especially for bio-magnetic measurements without any magnetic shielding at room temperature. In order to avoid a risk of traffic accident due to noise reduction electric vehicles, an alert system based on pico-Tesla MI sensor would be useful. Such system is suitable for building within a smart phone for easy use by pedestrians. Person-to-person direct magnetic telecommunications as hearing assistant for elderly is proposed for a new application of pico-Tesla MI sensor.

## References

[1] K. Mohri, "Application of amorphous magnetic wires to computer peripherals," *Materials Science and Engineering A—Structural Materials Properties Microstructure and Processing*, vol. 185, no. 1–2, pp. 141–145, 1994.

[2] L. V. Panina and K. Mohri, "Magneto-impedance effect in amorphous wires," *Appl. Phys. Lett.*, vol. 65, no. 9, pp. 1189–1191, 1994.

[3] L. V. Panina, K. Mohri, K. Bushida, and M. Noda, "Giant magneto-impedance and magneto-inductive effects in amorphous alloys," *J. Appl. Phys.*, vol. 76, no. 10, pp. 6198–6203, 1994.

[4] M. Noda, L. V. Panina, and K. Mohri, "Pulse response bistable magneto-impedance effect in amorphous wires," *IEEE Trans. Magn.*, vol. 31, no. 6, pp. 3167–3169, Jun. 1995.

[5] T. Kitoh, K. Mohri, and T. Uchiyama, "Asymmetrical magneto-impedance effect in twisted amorphous wires for sensitive magnetic sensors," *IEEE Trans. Magn.*, vol. 31, no. 6, pp. 3137–3139, Jun. 1995.

[6] K. Mohri, K. Bushida, M. Noda, H. Yoshida, L. V. Panina, and T. Uchiyama, "Magneto-impedance element," *IEEE Trans. Magn.*, vol. 31, no. 4, pp. 2455–2460, Apr. 1995.

[7] K. Mohri, L. V. Panina, T. Uchiyama, M. Noda, and K. Bushida, "Sensitive and quick response micro magnetic sensor utilizing magneto-impedance in co-rich amorphous wires," *IEEE Trans. Magn.*, vol. 31, no. 2, pp. 1266–1275, Feb. 1995.

[8] L. V. Panina, K. Mohri, T. Uchiyama, M. Noda, and K. Bushida, "Giant magneto-impedance in co-rich amorphous wires and films," *IEEE Trans. Magn.*, vol. 31, no. 2, pp. 1249–1260, Feb. 1995.

[9] L. V. Panina and K. Mohri, "Effect of magnetic structure on giant magneto-impedance in co-rich amorphous alloys," *J. Mag. Mag. Mat.*, vol. 158, pp. 137–140, 1996.

[10] V. P. Paramanov, A. S. Antonov, A. N. Lagarikov, L. V. Panina, and K. Mohri, "High frequency (1–1200 MHz) magneto-impeance in co-rich amorphous wires," *J. Appl. Phys.*, vol. 79, no. 8, pp. 6532–6534, 1996.

[11] L. V. Panina, K. Mohri, and T. Uchiyama, "Giant magneto-impedance in amorphous wire, single layer film and sandwich film," *Physica A*, vol. 241, no. 1–2, pp. 429–438, 1997.

[12] T. Yoshinaga, S. Furukawa, and K. Mohri, "Magneto-impedance effect in etched thin amorphous wires," *IEEE Trans. Magn.*, vol. 35, no. 5, pp. 3613–3615, May 1999.

[13] L. V. Panina, K. Mohri, and D. P. Makhnovskiy, "Mechanism of asymmetrical magneto-impedance in amorphous wires," *J. Appl. Phys.*, vol. 85, no. 8, pp. 5444–5446, 1999.

[14] K. Kawashima, I. Ogasawara, S. Ueno, and K. Mohri, "Asymmetrical magneto-impedance effect in torsion annealed co-rich amorphous wire for MI micro magnetic sensors," *IEEE Trans. Magn.*, vol. 35, no. 5, pp. 3610–3612, May 1999.

[15] T. Kanno, K. Mohri, T. Yagi, T. Uchiyama, and L. P. Shen, "Amorphous wire MI micro sensor using CMOS IC multivibrator," *IEEE Trans. Magn.*, vol. 33, no. 5, pp. 3353–3360, May 1997.

[16] N. Kawajiri, M. Kakabayashi, C. M. Cai, K. Mohri, and T. Uchiyama, "Highly stable MI micro sensor using CMOS IC multivibrator with synchronous rectification," *IEEE Trans. Magn.*, vol. 35, no. 5, pp. 3667–3669, May 1999.

[17] T. Uchiyama, K. Mohri, H. Itoh, K. Nakashima, J. Ouchi, and Y. Sudo, "Car traffic monitoring system using MI sensor buil-in disk set on the road," *IEEE Trans. Magn.*, vol. 36, no. 5, pp. 3670–3672, May 2000.

[18] C. M. Cai, K. Mohri, Y. Honkura, and M. Yamamoto, "Improved pulse carrier MI effect by flash anneal of amorphous wires and FM wireless CMOS IC torque sensor," *IEEE Trans. Magn.*, vol. 37, no. 4, pp. 2038–2041, Apr. 2001.

[19] C. M. Cai, K. Usami, M. Hayashi, and K. Mohri, "Frequency modulation type MI sensor using amorphous wire and CMOS inverter multivibrator," *IEEE Trans. Magn.*, vol. 40, no. 1, pp. 161–163, Jan. 2004.

[20] K. Mohri, T. Uchiyama, and L. V. Panina, "Magneto-impedance (MI) micro magnetic sensors—Principle and applications," *Transducers*, vol. 1, pp. 76–79, 1999.

[21] K. Mohri, T. Uchiyama, L. P. Shen, C. M. Cai, and L. V. Panina, "Sensitive micro magnetic sensor family utilizing magneto-impedance (MI) and stress-impedance (SI) effects for intelligent measurements and controls," *Sensors Actuators*, vol. A91, pp. 85–90, 2001.

[22] K. Mohri, T. Uchiyama, L. P. Shen, C. M. Cai, and L. V. Panina, "Amorphous wire and CMOS IC based sensitive micro magnetic sensors (MI sensor and SI sensor) for intelligent measurements and controls," *J. Mag. Mag. Mat.*, vol. 249, pp. 351–356, 2002.

[23] K. Mohri, T. Uchiyama, L. P. Shen, C. M. Cai, L. V. Panina, Y. Honkura, and M. Yamamoto, "Amorphous wire and CMOS IC based sensitive micromagnetic sensors utilizing magneto-impedance (MI) and stress-impedance (SI) effects," *IEEE Trans. Magn.*, vol. 38, no. 5, pp. 3063–3068, May 2002.

[24] K. Mohri and Y. Honkura, "Amorphous wire and CMOS IC based magneto-impedance sensors—Origin, topics, and future," *Sensor Lett.*, vol. 5, pp. 267–270, 2007.

[25] K. Mohri, F. B. Humphrey, L. V. Panina, Y. Honkura, J. Yamasaki, T. Uchiyama, and M. Hirami, "Advances of amorphous wire magnetics over 27 years," *Phys. Status Solidi A*, vol. 206, no. 4, pp. 601–607, 2009.

[26] K. Mohri, Y. Honkura, L. V. Panina, and T. Uchiyama, "Super MI sensor—Recent advances of amorphous wire CMOS IC magneto-impedance sensor," J. Nanoscience and Nanotechnology 2012, RTNSA issue, in press.

[27] T. Uchiyama, S. Nakayama, K. Mohri, and K. Bushida, "Biomagnetic field detection using very high sensitivity magneto-impedance sensors for medical applications," *Phys. Status Solidi A*, vol. 206, no. 4, pp. 639–643, 2009.

[28] K. Mohri, T. Uchiyama, M. Yamada, T. Watanabe, Y. Inden, T. Kato, and S. Iwata, "Arousal effect of physiological magnetic stimulation on elder person's spine for prevention of drowsiness during car driving," *IEEE Trans. Magn.*, vol. 47, no. 10, pp. 3066–3069, Oct. 2011.

[29] K. Mohri, Y. Nakamura, T. Uchiyama, Y. Mohri, Yu. Mohri, and Y. Inden, "Sensing of human micro-vibration transmitted along solid using pico-tesla magneto-impedance sensor (pT-MI sensor)," *Piers Online*, vol. 6, no. 2, pp. 161–164, 2010.

[30] T. Uchiyama, K. Mohri, and S. Nakayama, "Measurement of spontaneous oscillatory magnetic field of guinea-pig smooth muscle preparation using pico-tesla resolution amorphous wire magneto-impedance sensor," *IEEE Trans. Magn.*, vol. 47, no. 10, pp. 3066–3069, Oct. 2011.

[31] K. Mohri, M. Fukushima, Y. Mohri, and Yu. Mohri, "Detection of magnetization of 6 Hz, 10 $\mu$T magnetic field applied water using PT-MI sensor," *Piers Online*, vol. 6, no. 2, pp. 145–148, 2010.

[32] N. Hamada, A. Shimode, T. Kawano, H. Arakawa, M. Yamamoto, and Y. Honkura, "Development of low noise GMI sensor and its applications," in *Proc. Intermag*, 2011, FF-08.

[33] K. Mohri, T. Uchiyama, M. Yamada, Y. Mohri, K. Endo, T. Suzuki, and Y. Inden, "Physiological magnetic stimulation for arousal of elder car driver evaluated with electro-encephalogram and spine magnetic field," in *Proc. Intermag*, 2012, ED-04.

[34] L. G. C. Melo, D. Menard, A. Yelon, L. Ding, S. Saez, and C. Dolabdjian, "Optimization of the magnetic noise and sensitivity of giant magnetoimpedance sensors," *J. Appl. Phys.*, vol. 103, pp. 033903-1–03303-6, 2008.

[35] Y. Adachi, J. Kawai, M. Miyamoto, H. Ogata, M. Tomori, S. Kawabata, T. Sato, and G. Uehara, "A SQUID system for measurement of spinal cord evoked field of supine subjects," *IEEE Trans. Appl. Supercond.*, vol. 19, no. 3, pp. 861–866, Jun. 2009.

[36] S. Tomizawa, S. Kawabata, S. Komori, H. Hoshino, Y. Fukuoka, and K. Shinomiya, "Evaluation of segmental spinal cord evoked magnetic field after sciatic nerve stimulation," *Clin. Neurophys.*, vol. 119, no. 5, pp. 1111–1118, 2008.

[37] S. Simpson, "Are hybrid cars too quiet to be safe for pedestrians?," *Sci. Amer.*, Jul. 30, 2008.